Phase retrieval tomography in the presence of noise

Citation:
Arhatari, B.D., Gates, W.P., Eshtiaghi, N. and Peele, A.G. 2010, Phase retrieval tomography in the presence of noise, *Journal of applied physics*, vol. 107, no. 3, 034904, pp. 1-7.

DOI: http://www.dx.doi.org/10.1063/1.3298930

Phase retrieval tomography in the presence of noise

B. D. Arhatari,[1,a)] W. P. Gates,[2] N. Eshtiaghi,[3] and A. G. Peele[1]
[1]*Physics Department, La Trobe University, Victoria 3086, Australia*
[2]*Civil Engineering Department, Monash University, Victoria 3800, Australia*
[3]*Chemical Engineering Department, Monash University, Victoria 3800, Australia*

(Received 13 July 2009; accepted 4 January 2010; published online 4 February 2010)

We describe the use of single-plane phase retrieval tomography using a laboratory-based x-ray source, under conditions where the retrieval is not formally valid, to present images of the internal structure of an Aerosil granule and a hydrated bentonite gel. The technique provides phase images for samples that interact weakly with the x-ray beam. As the method is less affected by noise than an alternative two-plane phase retrieval method that is otherwise formally valid, object structure can be observed that would not otherwise be seen. We demonstrate our results for phase imaging in tomographic measurements. © *2010 American Institute of Physics*. [doi:10.1063/1.3298930]

I. INTRODUCTION

In conventional or absorption, tomography, the distribution of x-ray attenuation by the object can be calculated using filtered backprojection[1] from contact, or radiological, measurements of the intensity as modulated by the sample for a set of different projections through the sample.[2] This can become a problem for materials with low electron density due to the weak attenuation of x-rays where noise in the experimental system can swamp the signal due to absorption. In such cases it has been recognized that measurement of the propagated beam exiting a sample will exhibit contrast due to diffraction from the spatial distribution of the real and imaginary parts of the refractive index of a material. The imaginary part of the refractive index is colloquially associated with absorption imaging while the real part can dominate what is referred to phase contrast imaging.[3] Standard filtered backprojection methods[2] can be applied to the projections acquired in phase contrast imaging to provide a qualitative picture of the sample due, typically, to edge enhancement of the sample image.[4] *Phase contrast* methods have been widely used by synchrotron researchers due to the highly coherence of the source.[5] However, laboratory-based x-ray tube systems with sufficiently small source sizes have also been used to demonstrate phase contrast imaging.[6,7]

There are several approaches to phase retrieval currently used.[8–11] We consider here methods that rely solely on the free-space propagation of x-rays that exit a sample as this allows sample imaging with a minimum of additional equipment. There are also several algorithms that have been explored for free-space propagation[8–10] and the particular method chosen will depend on the imaging regime in which the data has been acquired. This will include factors such as the x-ray energy used, the properties of the sample and the experimental geometry. An important class of algorithms, in the context of free-space propagation methods, are those where the assumption is made that the sample is homogeneous.[10,12] For more general samples multiple planes of image data at different propagation distances must be collected in order to solve the phase retrieval problem. Under the assumption of sample homogeneity a single plane of data will typically suffice and hence these methods are often referred to as single-plane methods.

In phase retrieval tomography, the intensity data measured at the detector is subjected to a phase retrieval step that provides a map of the real part of the projected refractive index through the sample. Those projections can in turn be operated on using filtered backprojection to obtain the three-dimensional (3D) distribution.[8,13] Alternatively, algorithms have been demonstrated that combine the phase retrieval and filtered backprojection steps into a single operation that produce a 3D map of the sample distribution in the real part of the refractive index.[14–16] In some of that work,[16,17] it was shown that, although violating the assumption of homogeneity, useful results could still be obtained for nonhomogeneous samples when using a single-plane method.

In this paper, we will further explore the use of a particular single-plane approach under conditions that violate the assumption of sample homogeneity in the context of phase imaging using a laboratory source. We demonstrate that notwithstanding the lack of sample homogeneity high-quality images amenable for 3D sample segmentation can be obtained. In addition, due to the different noise characteristics of the single-plane method compared to some multiple-plane methods, more useful images can be obtained using the single-plane approach for nonhomogeneous samples. Some experimental results of this type of phase retrieval will be demonstrated.

II. PHASE RETRIEVAL, NOISE, AND HOMOGENEITY

A well-studied multiple-plane phase retrieval method[3] can be written as

$$\varphi(\boldsymbol{r}) = -k\nabla^{-2}\left(\nabla\cdot\left\{\frac{1}{I(\boldsymbol{r})}\nabla\left[\nabla^{-2}\frac{\partial I(\boldsymbol{r})}{\partial z}\right]\right\}\right), \tag{1}$$

where $k=2\pi/\lambda$, λ is the wavelength, $\boldsymbol{r}$ is the position in a plane, I is the intensity, z is the propagation distance, and φ is the retrieved phase. Note that in the Fourier domain, the Laplacian has a simple expression given by ∇^{-2}

a)Electronic mail: b.arhatari@latrobe.edu.au.

$=-\mathbb{F}^{-1}(1/\boldsymbol{u}^2)\mathbb{F}$ and the grad term by $\nabla=-\mathbb{F}^{-1}\boldsymbol{u}\mathbb{F}$ so that

$$\varphi(\boldsymbol{r}) = -k\mathbb{F}^{-1}\frac{1}{\boldsymbol{u}^2}\boldsymbol{u}\mathbb{F}\frac{1}{I(\boldsymbol{r})}\mathbb{F}^{-1}\boldsymbol{u}\frac{1}{\boldsymbol{u}^2}\mathbb{F}\frac{\partial I(\boldsymbol{r})}{\partial z}, \tag{2}$$

where $\mathbb{F}$ is the Fourier transform operator and $\boldsymbol{u}$ is the Fourier variable conjugate to the position coordinates. Two intensity images taken at different propagation distances separated by dz are needed for this method in order to obtain the intensity derivative, $\partial I/\partial z$, hence its classification as a multiple-plane, or in this case two-plane, scheme. It is readily seen that low spatial frequencies in the intensity derivative and in the filtered intensity derivative divided by the intensity will be enhanced by the 1/u filtering term that appears twice in the solution to the phase. Consequently, any noise signal that has power at low spatial frequencies will be enhanced in the retrieved phase.

The phase retrieval for a single-plane method is written[12,14] (in the weakly absorbing limit)

$$\varphi(\boldsymbol{r}) = -k\delta\mathbb{F}^{-1}\left(\frac{1}{\mu+z\delta\boldsymbol{u}^2}\mathbb{F}\left[\frac{I^z(\boldsymbol{r})}{I^{in}(\boldsymbol{r})}-1\right]\right), \tag{3}$$

where μ and δ are the attenuation coefficient and the decrement of the real part of the refractive index, respectively, I^z is the intensity at a distance z and I^{in} is the intensity entering the sample. It can be seen here that low spatial frequencies will now be suppressed by the appearance of the absorption term, μ, in the denominator.

To better compare the noise performance of the two approaches, consider the case when μ varies insignificantly in $\boldsymbol{r}$ direction. So that $\partial\mu/\partial r\approx 0$ and Eq. (2) can be simplified as

$$\varphi(\boldsymbol{r}) = -\frac{k}{I}\mathbb{F}^{-1}\frac{1}{\boldsymbol{u}^2}\mathbb{F}\frac{\partial I(\boldsymbol{r})}{\partial z}. \tag{4}$$

Figure 1 shows the simulation result of applying the two- and single-plane phase retrieval of Eqs. (2) and (3) to a Gaussian shaped phase object with maximum phase shift of 4.7 rad. The noise is composed of random numbers with a standard deviation of a percentage of the mean intensity. We chose experimental and materials parameters for an experiment similar to those described below to illustrate the noise behavior here. The x-ray energy was 11.5 keV. We used a polyimide sample ($C_{22}H_{10}N_2O_4$) with $\delta=2.36\times10^{-6}$ and $\mu=355\ \mathrm{m}^{-1}$. The noise is 1%. The separation distance, dz, for the two-plane method and the propagation distance, z, for the one-plane method are shown in the first column of Fig. 1. The plots are taken horizontally in the middle of the field of view $1000\times1000\ \mu\mathrm{m}^2$ of each image. Figure 1 shows that the single-plane algorithm is more stable to noise and increasing distance can be used to reduce the noise effect in both single- and two-plane phase retrieval methods.

If we consider measured intensity that is entirely comprised of noise, $n(\boldsymbol{r})$, then it is readily shown[18] that the characteristic features in the retrieved phase obtained from Eq. (4) can be described by

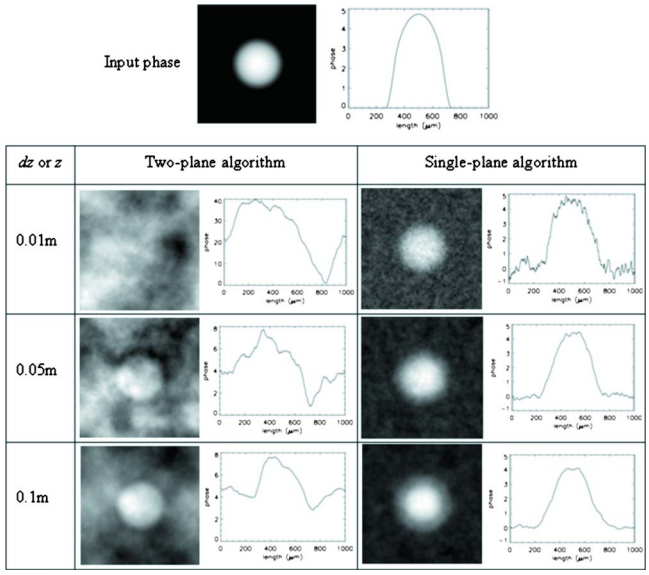

FIG. 1. (Color online) Simulation results of phase reconstruction of a phase object with 1% noise using the two-plane [Eq. (2)] and single-plane [Eq. (3)] algorithms, respectively. The input phase is shown on the top part. The distance shown is dz for the two-plane method and z for the single-plane method. For each method and distance an image of the retrieved phase and a lineout horizontally through the center showing magnitudes is shown. Additionally, it is also apparent that the same amount of noise will give less effect for the single-plane approach than for the two-plane approach.

$$\varphi^2_{\mathrm{noise}}(\boldsymbol{r}) = -\mathbb{F}^{-1}\frac{k\sqrt{2}}{I\cdot\boldsymbol{u}^2}\frac{\mathbb{F}n(\boldsymbol{r})}{dz}, \tag{5}$$

where the superscript symbol 2 denotes that the phase is retrieved using the two-plane method described in Eqs. (2) and (4). It can be similarly shown that the phase retrieved from a noise signal using the single-plane method of Eq. (3) is given by

$$\varphi^1_{\mathrm{noise}}(\boldsymbol{r}) = -\mathbb{F}^{-1}\frac{k\delta}{\mu+z\delta\boldsymbol{u}^2}\mathbb{F}n(\boldsymbol{r}), \tag{6}$$

where the superscript symbol 1 denotes the single-plane method.

For a noise distribution of pseudorandom numbers, $n(\boldsymbol{r})$, the Fourier transform, is also composed of random numbers. Equation (5) then shows that the distribution of spatial frequencies in the retrieved phase arising from noise is strongly peaked at the origin due to the effect of the division by $\boldsymbol{u}^2$. Thus this type of phase retrieval behaves as a low pass filter with a strong peak around the origin.[18] The result is that low frequency noise is amplified, which causes a low frequency contamination in the phase retrieved product, as confirmed in simulation results (Fig. 1 left column). Equation (5) also shows that a large separation distance between the two measurement planes, dz, is critical for reducing the magnitude of noise as can be seen from the lineouts in the left column of Fig. 1.

For the single-plane method Eq. (6) shows that the distribution of spatial frequencies in the retrieved phase arising from noise will have a similar distribution to the original random number noise, provided the attenuation term, μ, in the denominator, $\mu+z\delta\boldsymbol{u}^2$ dominates significantly. As the

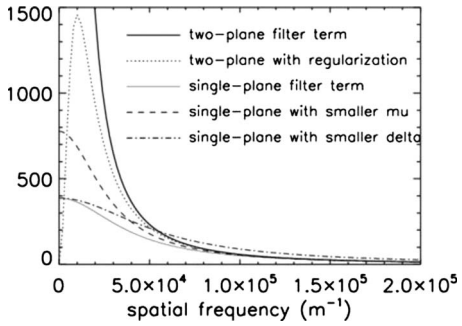

FIG. 2. Plot showing the filter term from Eq. (5), $k/(zu^2)$ (thick solid line) and from Eq. (6) $(k\delta)/(\mu+z\delta u^2)$ (thin solid line) as a function of spatial frequency. The dotted line shows Eq. (5) with a Tikhonov regularization parameter. The dashed and dashed-dotted lines are for Eq. (6) but where the attenuation term, μ, and the phase term, δ, have been decreased by a factor of 2, respectively.

propagation distance, z, increases the filter acts more like a low pass filter but where the attenuation component will always limit the amplification at the origin (Fig. 1 right column). It can also be seen from the lineouts in Fig. 1 that the magnitude of the retrieved phase due to noise for the single-plane method is, in this case, less than that for the two-plane method.

A Tikhonov regularization parameter, α, that handles division by $u=0$ in Eq. (5) can also act to provide noise suppression by substituting[19]

$$\frac{1}{u^2} \rightarrow \frac{u^2}{(u^2+\alpha^2)^2}. \tag{7}$$

Tikhonov regularization has been pointed out before in the context of the division by zero effect that the filter term introduces in various forms of phase retrieval[10] but it is worth considering here in relation to the effects of noise and the quality of the retrieval.

Figure 2 shows the comparison of the filter terms for Tikhonov regularization, for the two-plane approach and for the single-plane approach. For realistic parameters it can be seen that the single-plane approach will limit low frequency noise effects compared to the two-plane approach. Violating the homogeneity assumption will have a similar effect to using the wrong materials parameters, δ and μ in Eq. (3). The effect of this on the filter term can be seen in Fig. 2. It can be seen that even a gross change (factor of two in the absorption coefficient or δ value) has relatively little effect on the filter term in the phase retrieval. Additionally, while having the wrong δ and μ for nonhomogenous samples will give incorrect magnitudes in the retrieved phase. The relatively small errors at low frequency mean that, in general, the retrieved shape of an object will be preserved. On the other hand, varying the Tikhonov regularization parameter, α, for the two-plane approach, will suppress very low frequency terms as shown in Fig. 2 (dotted line). Increasing the value of the regularization parameter will shift the maximum peak to higher frequencies and will suppress more of the low frequency terms. Therefore, Tikhonov regularization is more likely to introduce artifacts into the retrieved shape of an object.

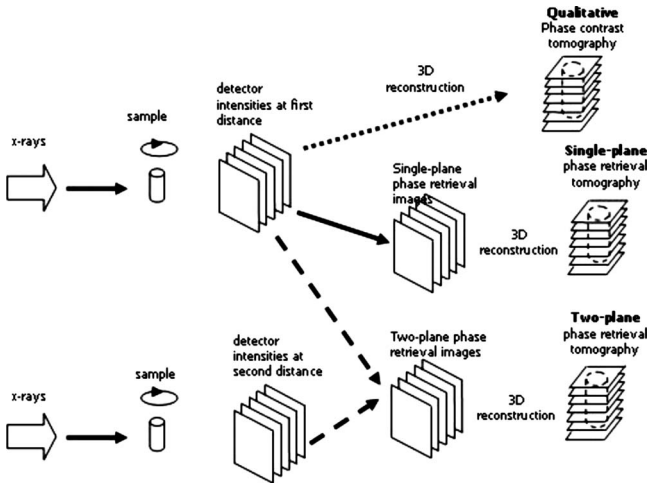

FIG. 3. Process diagram to produce qualitative-(dotted arrow), single-plane-(solid arrow) and two-plane-(dash arrow) tomography results. In qualitative phase tomography phase contrast images at one distance are collected and tomographically reconstructed to produce an edge-enhanced image. In single-plane phase tomography phase contrast images at one distance are collected, single-plane phase retrieval is applied (even though the requirement for sample homogeneity is violated) and the resulting phase images are tomographically reconstructed to produce a phase map of the sample. In two-plane phase tomography phase contrast images at two distances are collected, two-plane phase retrieval is applied and the resulting phase images are tomographically reconstructed to produce a phase map of the sample.

Overall, violating homogeneity is thus expected to have a relatively benign effect on the retrieved phase in the single-plane approach compared to the noise and shape effects seen in the two-plane approach.

III. EXPERIMENTAL RESULTS

We present here two case studies comparing qualitative phase contrast tomography (i.e., no phase retrieval), single-plane phase retrieval tomography where we violate the assumption of object homogeneity and two-plane phase retrieval tomography. The three different cases are represented schematically in Fig. 3.

The first sample is an aerosil granule representing a weakly absorbing nonhomogeneous sample. The second sample is a hydrated bentonite gel representing an absorbing and nonhomogeneous sample.

A. Aerosil granule: Nonhomogeneous sample

Aerosil R202 (Degussa Co. Germany) is the commercial name for highly hydrophobic fumed silica. Fumed silica is an amorphous compound of silicon dioxide (sand) produced in high-temperature processes. Aerosil R202 is a fine, very light, and white powder with a particle size of around 16 nm and is widely used in the cosmetic and pharmaceutical industries. Granulation of hydrophobic powders is frequently required in the pharmaceutical industry.[20] Granulation is the process of collecting particles together by creating bonds between them by using a binding agent.[21] The poor wetting properties of hydrophobic powders can create considerable difficulty in understanding, controlling, and trouble-shooting these industrial granulation processes.[20] Hollow granule for-

mation is a new way to solve the problematic granulating behavior of hydrophobic powders.[21] The dissolution rate of tablets due to the presence of hollow granules will be rapid and the drying will be fast due to the thin shell thickness. These granules also show good compressibility characteristics during the tablet pressing process. Hollow granules can be formed from hydrophobic powders by spreading powder around a template drop and the subsequent drying of the interior liquid to form a hollow granule. This process is known as *liquid marble* or *dry water*.[20]

This sample represents a weakly absorbing nonhomogeneous material. 3D x-ray images of a hollow Aerosil granule were obtained using the x-ray microcomputed tomography machine (Xradia Inc. USA), located in the Physics Department, La Trobe University. An x-ray source with a Tungsten target was operated at 40 kV and a current of 150 μA. The source size is about 8 μm. The illuminating spectrum with such a source is not monochromatic, as is assumed in the phase retrieval formulae discussed above. We used an effective wavelength matched to the phase and absorption components in the formula using the procedure developed by Arhatari *et al.*[22] This approach works best for samples that are weakly absorbing. Consequently, we have applied the approach here to both a weakly (this sample) and strongly absorbing sample (the second sample) to investigate whether the beneficial effect in noise suppression still applies when the sample is both inhomogeneous and strongly absorbing.

The granule was scanned by acquiring 361 projections taken at 0.5° rotational increments. The distance between the source and sample was $z_{ss}=100$ mm, and the sample detector distances were $z_{sd}=20$ and 125 mm. In this point projection geometry the phase retrieval formulae are modified by replacing distances with effective distance[12] calculated by $z_{eff}=(z_{ss}z_{sd})/(z_{ss}+z_{sd})=16.7$ mm and 55.6 mm and by scaling images by the magnification, which was here 1.2 and 2.25. The exposure time was 60 s for each projection. A charge coupled device camera coupled with a scintillator and a 20× objective lens was used as the detector. The best resolution for this setup was about 1.2 μm. A data set of intensity projections at the two propagation distances was obtained and the three types of tomographic reconstructions described in Fig. 3 were calculated.

Figure 4 shows the result for qualitative phase tomography. The edge-contrast characteristic of phase contrast imaging in Fig. 4 shows that the Aerosil granule is spherical and hollow with a diameter of about 200 μm. It has a thin (2–4 μm) shell and there are spongelike structures outside the granule of similar density to the shell. The images at 16.7 mm show better resolution due to the source size demagnification by the geometric setup. Blurring from the finite source size starts to influence the images taken at 55.6 mm, as indicated by the thicker and blurrier shell features.

Phase retrieval tomography becomes an important technique for the study of the 3D morphology and structure of hollow granules within Aerosil, as qualitative phase contrast tomography (Fig. 4) does not completely show the information available from the sample. Accordingly, we performed two-plane phase retrieval for each projected set of data (taken at 16.7 and 55.6 mm with a separation in effective

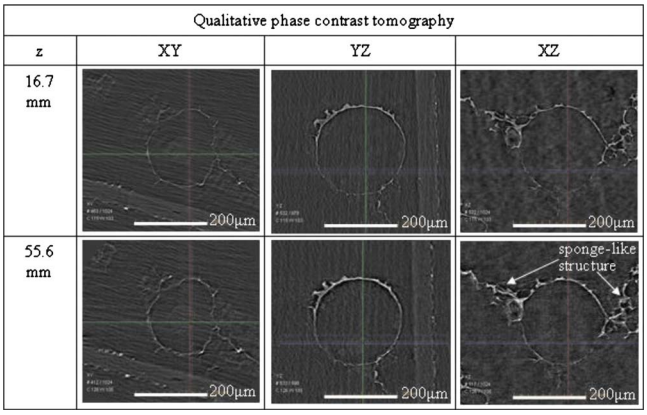

FIG. 4. (Color online) Qualitative phase contrast tomography of an Aerosil hollow granule, taken at effective propagation distances of 16.7 and 55.6 mm. Cross section planes XY, YZ, and XZ are indicated.

propagation distance of 38.9 mm) thus producing phase images for each projection. The resulting 3D reconstruction is shown in Fig. 5 in the same cross section planes as for Fig. 4. Figure 5 shows similar spherical wall structure as the image in Fig. 4, albeit indicating thicker walls. This is expected as Fig. 5 shows a map of the phase and Fig. 4 essentially shows a map of the Laplacian of the phase. Of more interest is the suggestion of an object inside the spherical shell. However, the images are contaminated by low frequency noise artifacts, as indicated by a layer of clouds on the image and these are at a similar level of intensity to the putative object.

Finally we performed single-plane phase retrieval for each projected set of data at both propagation distances. We used the refractive index of silicon dioxide [density of 2.2 g/cm^3 at effective energy for the attenuation term of 10.5 keV and for the δ term of 11.5 keV (Ref. 22)] to calculate the phase in each projection. The resulting 3D reconstruction is shown in Fig. 6 in the same cross section planes as for Fig. 4. The single-plane algorithm clearly reveals better sample structure and also provides greater contrast. While the 16.7 mm result provides better high frequency contrast, it is more sensitive to noise, compared to the larger propagation distance of 55.6 mm as indicated by the presence of noise artifacts. This is in agreement with Fig. 1 (right column) that larger propagation distances will provide a lower noise magnitude in the retrieved result.

Of particular interest is that the putative object seen in Fig. 5 is clearly revealed in Fig. 6. The results of the single-plane phase retrieval (Fig. 6) are consistent with the features observed in a scanning electron microscopy (SEM) micro-

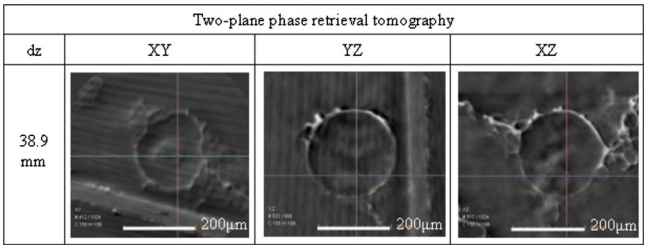

FIG. 5. (Color online) Phase retrieval tomography of an Aerosil hollow granule, based on the two-plane phase retrieval algorithm.

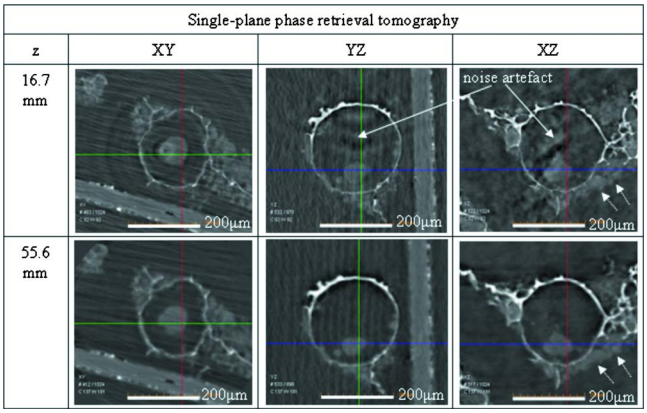

FIG. 6. (Color online) Single-plane phase retrieval tomography of an Aerosil hollow granule.

graph (Fig. 7). The micrograph shows multiple small, spherical attachments on the surface of the granule (indicated by arrows in Fig. 7). But it is not possible to tell from the micrograph whether the attachments are small hollow granules or small aggregates of the primary particles. The single-plane phase retrieval result confirms that the attachments (indicated by dot arrows in Fig. 6 right column) are not hollow. The bright outlines surrounding the granule shell indicates a denser wall structure formed from Aerosil and the binder (i.e., HPC-Hydroxyl Propyl Cellulose), while the weak white color is the agglomerated Aerosil. Aerosil powder tends to self-agglomerate to form a larger particle size between 1 and 50 μm. These facts and the images suggest that these small exterior attachments are aggregated Aerosil particles.[21]

This similarity between the external structures and the internal structures in Fig. 6 also suggests that the large spherical hollow granule contains smaller spherical aggregates of Aerosil powder. The internal aggregates may be formed during granulation or perhaps are related to erosion of the interior of the granule shell during drying, transportation, or other handling process.[21]

B. Hydrated bentonite gel: Nonweak absorption and nonhomogeneous sample

Bentonite is a naturally occurring material and is among the most important industrial minerals used in energy recovery, manufacturing, and environmental industries.[23] Bentonites are composed predominantly of the swelling clay mineral montmorillonite, but other minerals, such as quartz, feldspars, micas, and carbonates may also be present in the fine fraction. Swelling clay minerals like montmorillonite can take up several times their mass in water and swell to several times their volume, and when confined transmit water very slowly. Because of this, bentonites are useful as natural seals in dams, or as secondary barriers in landfills.[23] An important issue in the use of bentonites as hydraulic barriers is salinity induced loss of gel structure. When fully hydrated sodium saturated montmorillonite forms a gel which strongly attenuates water movement. However, because montmorillonite surfaces interact strongly with solutes, when exposed to saline water, or water containing a large proportion of divalent cations,[24] the gel structure collapses forming micron-sized pores which are not as effective at retaining water. While various spectroscopic and physical measures can be correlated with changes in the pore sizes, there are few direct measures available. Electron microscopy techniques have been developed[25] but are time consuming and can be subject to experimental artifact or beam damage. Scanning transmission x-ray spectromicroscopy[26] methods are useful for gaining high resolution images, but suffer from difficulty in gaining experimentally relevant information. For example, samples have to be of submicron to a few microns thick to provide quantitative results, providing obvious difficulty in studying gel structures. Thus, it is expected that 3D tomography can provide a visual indication of the changes in gel structure occurring when an intact bentonite sample is subjected to wetting by different liquids.

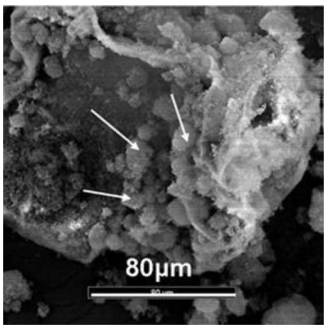

FIG. 7. SEM micrograph image of Aerosil granule attached by multiple small, spherical particles (Ref. 21).

A processed sodium bentonite powder from Miles, Queensland, Australia, (marketed as Trugel® by UniMin Australia) was used. We immersed a sample of bentonite within solutions of deionised water of 0.2*M* $CaCl_2$ to determine the effectiveness of 3D tomography to differentiate differences in pore features within the clay gels. In its bulk form, essentially all of the bentonite passes a 100 μm sieve, but this is composed of a range of particle sizes and different mineral phases.[27] The bulk material is composed of montmorillonite (69%), quartz (15%), opaline silica (7%), feldspar (8%), and minor amounts (~1%) of mica, zeolite, gypsum, and anatase. Importantly, the <0.2 μm (200 nm) fraction, which makes up 50% of the bulk material, is 97% montmorillonite with a small amount of opaline silica.

The clay-gel sample immersed in $CaCl_2$ was chosen to represent both a nonhomogeneous and absorbing sample. A similar setup as described above was used, except that a tube voltage of 100 kV and exposure time of 80 s was used for each projection. The number of projections acquired for this scan was 721 taken at 0.25° increments. A data set of intensity projections, at the same two effective propagation distances as before were obtained and the three types of tomographic reconstructions described in Fig. 3 were calculated.

Figure 8 shows the result for qualitative phase tomography. From the slice image, we can see that the sample consists mainly of particles within the 5–20 μm size range. Some of them are much larger, on the order of 200 μm, as seen in upper right of the YZ plane. As is typical for quali-

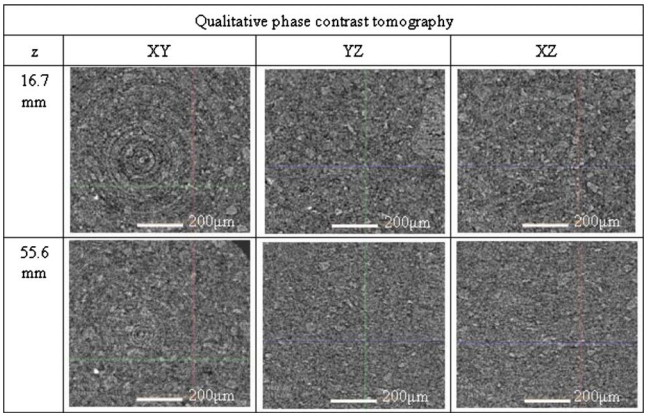

FIG. 8. (Color online) Qualitative phase contrast tomography of a hydrated bentonite gel immersed in 0.2*M* $CaCl_2$, taken at propagation distances of 16.7 and 55.6 mm. Cross section planes XY, YZ, and XZ are indicated.

tative tomography, edge enhancement from all the particles is well defined and the images at 16.7 mm have better resolution than those at 55.6 mm.

We performed two-plane phase retrieval for each projected set of data (taken at 16.7 and 55.6 mm with a separation in effective propagation distance of 38.9 mm) thus producing phase images for each projection. The resulting 3D reconstruction is shown in Fig. 9 in the same cross section planes as for Fig. 8. However, the images shown in Fig. 9 have very poor contrast, because the low frequency artifacts completely dominate the result.

Finally we performed single-plane phase retrieval for each projected set of data at both propagation distances. We used the refractive index of clay (with density of 1.3 g/cm^3) to calculate the phase in each projection. The resulting 3D reconstruction is shown in Fig. 10 in the same cross section planes as for Fig. 8. Notwithstanding the violation of weak absorption (as well as homogeneity) it can be seen that the resulting images provide well resolved and high contrast features that can potentially be used to segment the different regions of the image. As observed in the qualitative phase analysis, immersion of the bentonite in 0.2*M* $CaCl_2$ caused flocculation of the gel phase (best observed at the 55.6 mm distance in Fig. 10). The white specks (circled in the XY view) are most likely anatase grains, whereas the intermediate density particles (circled in the YZ view) are quartz grains. Individual flocs of clay are observed, as these are large incompletely hydrated particles, and the flocs are often separated by mineral free void spaces (represented in black). This result is expected for a material consisting of a mixture

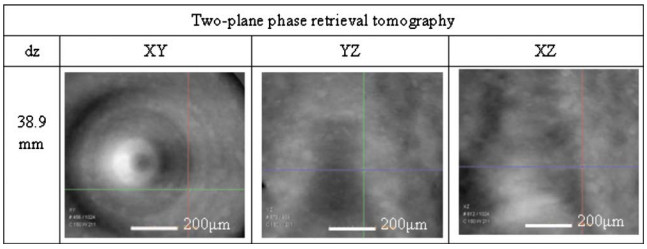

FIG. 9. (Color online) Two-plane phase retrieval tomography of a hydrated bentonite gel immersed in 0.2*M* $CaCl_2$.

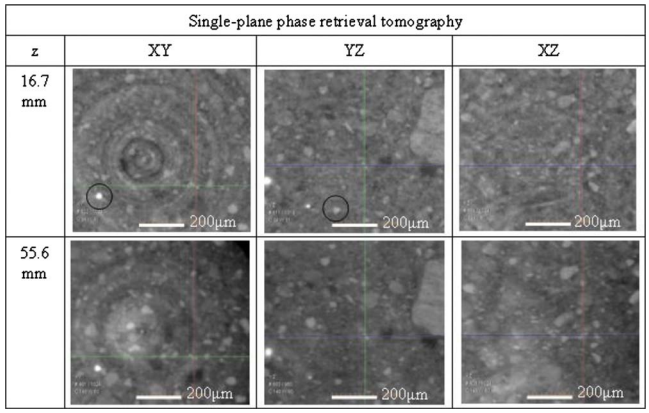

FIG. 10. (Color online) Single-plane phase retrieval tomography of a hydrated bentonite gel immersed in 0.2*M* $CaCl_2$.

of nonswelling dense mineral phases (e.g., quartz, feldspar, and other impurities) dispersed within a matrix composed predominantly of partially swollen and flocculated montmorillonite. The large particle at the upper right of the YZ plane shows a distinct boundary with the matrix material and has a greater density than most of the bentonite gel but also lower density than the many smaller quartz particles (e.g., circled particle in the YZ image). We interpret this particle as being an incompletely hydrated bentonite particle, as it is too large to be a single grain of any accessory mineral. These features are not observed in images of bentonite when it is immersed in deionised water.

IV. CONCLUSION

Single-plane phase retrieval tomography appears to be a powerful technique that can provide useful phase images of nonhomogeneous and either weakly or strongly absorbing materials, due to its nonsensitivity to noise. In particular, we have shown that these results can be successfully carried out using an x-ray laboratory-based source. The resulting images are far cleaner in terms of noise artifacts than the same data analyzed using the (formally valid) two-plane retrieval method. While such results are not quantitative due to the violations of the assumptions used in the methods the errors appear to be relatively small and well behaved in the sense that they do not produce image artifacts. Accordingly, data produced using this method will be very useful in segmenting samples into regions of different composition.

ACKNOWLEDGMENTS

The authors acknowledge the support of the Australian Research Council through the Centre of Excellence for Coherent X-ray Science and by an APDI fellowship (BDA), and Monash University for an Engineering Faculty New Staff Research Grant (WPG).

[1]G. T. Herman, *Image Reconstruction from Projections* (Springer-Verlag, Berlin, 1979).
[2]A. C. Kak and M. Slaney, *Principles of Computerized Tomographic Imaging* (IEEE, New York, 1988).
[3]D. M. Paganin, *Coherent X-Ray Optics* (Oxford University Press, New York, 2006).
[4]S. C. Mayo, T. J. Davis, T. E. Gureyev, P. R. Miller, D. Paganin, A.

Pogany, A. W. Stevenson, and S. W. Wilkins, Opt. Express **11**, 2289 (2003).
[5]A. Snigirev, I. Snigreva, V. Kohn, S. Kuznetsov, and I. Schelokov, Rev. Sci. Instrum. **66**, 5486 (1995).
[6]S. W. Wilkins, T. E. Gureyev, D. Gao, A. Pogany, and A. W. Stevenson, Nature (London) **384**, 335 (1996).
[7]B. D. Arhatari, A. P. Mancuso, A. G. Peele, and K. A. Nugent, Rev. Sci. Instrum. **75**, 5271 (2004).
[8]P. Cloetens, W. Ludwig, J. Baruchel, D. Van Dijck, J. Van Landuijt, J. Guigay, and M. Schlenker, Appl. Phys. Lett. **75**, 2912 (1999).
[9]K. A. Nugent, T. E. Gureyev, D. F. Cookson, D. Paganin, and Z. Barnea, Phys. Rev. Lett. **77**, 2961 (1996).
[10]L. D. Turner, A. G. Peele, B. Dhal, A. P. Mancuso, R. E. Scholten, C. Q. Tran, K. A. Nugent, J. P. Hayes, and D. Paterson, Opt. Express **12**, 2960 (2004).
[11]J. N. Clark, G. J. Williams, H. M. Quiney, L. Whitehead, M. D. d. Jonge, E. Hanssen, M. Altissimo, K. A. Nugent, and A. G. Peele, Opt. Express **16**, 3342 (2008).
[12]D. Paganin, S. Mayo, T. E. Gureyev, P. R. Miller, and S. W. Wilkins, J. Microsc. (Paris) **206**, 33 (2002).
[13]P. J. McMahon, A. G. Peele, D. Paterson, J. J. A. Lin, T. H. K. Irving, I. McNulty, and K. A. Nugent, Opt. Commun. **217**, 53 (2003).
[14]B. D. Arhatari, F. De Carlo, and A. G. Peele, Rev. Sci. Instrum. **78**, 053701 (2007).
[15]A. V. Bronnikov, Opt. Commun. **171**, 239 (1999).
[16]A. Groso, R. Abela, and M. Stampanoni, Opt. Express **14**, 8103 (2006).
[17]T. Weitkamp, A. Diaz, C. David, F. Pfeiffer, M. Stampanoni, P. Cloetens, and E. Ziegler, Opt. Express **13**, 6296 (2005).
[18]D. Paganin, A. Barty, P. J. McMahon, and K. A. Nugent, J. Microsc. **214**, 51 (2004).
[19]A. N. Tikhonov, Sov. Math. Dokl. **4**, 1035 (1963).
[20]K. P. Hapgood and B. Khanmohammadi, Powder Technol. **189**, 253 (2009).
[21]N. Eshtiaghi, B. D. Arhatari, and K. P. Hapgood, Adv. Powder Technol. **20**(6), 558 (2009).
[22]B. D. Arhatari, K. Hannah, E. Balaur, and A. G. Peele, Opt. Express **16**, 19950 (2008).
[23]W. P. Gates, A. Bouazza, and G. J. Churchman, Elements **5**(2), 105 (2009).
[24]D. A. Laird, Appl. Clay Sci. **34**, 74 (2006).
[25]D. Tessier and G. Pedro, Proceedings of the International Clay Conference, Denver, 1987 (unpublised).
[26]B. P. Tonner, T. Droubay, J. Denlinger, W. Meyer-Ilse, T. Warwick, J. Rothe, E. Kneedler, K. Pecher, K. Nealson, and T. Grundl, Surf. Interface Anal. **27**, 247 (1999).
[27]W. P. Gates, J. S. Anderson, M. D. Raven, and G. J. Churchman, Appl. Clay Sci. **20**, 189 (2002).